University Library

A gateway to Melbourne's research publications

Minerva Access is the Institutional Repository of The University of Melbourne

Author/s:
Atkinson, SC;Dogovski, C;Downton, MT;Czabotar, PE;Dobson, RCJ;Gerrard, JA;Wagner, J;Perugini, MA

Title:
Structural, kinetic and computational investigation of Vitis vinifera DHDPS reveals new insight into the mechanism of lysine-mediated allosteric inhibition

Date:
2013-03-01

Citation:
Atkinson, S. C., Dogovski, C., Downton, M. T., Czabotar, P. E., Dobson, R. C. J., Gerrard, J. A., Wagner, J. & Perugini, M. A. (2013). Structural, kinetic and computational investigation of Vitis vinifera DHDPS reveals new insight into the mechanism of lysine-mediated allosteric inhibition. Plant Molecular Biology, 81 (4-5), pp.431-446. https://doi.org/10.1007/s11103-013-0014-7.

Persistent Link:
https://hdl.handle.net/11343/282680

Title

Structural, Kinetic and Computational Investigation of *Vitis vinifera* DHDPS Reveals New Insight into the Mechanism of Lysine-Mediated Allosteric Inhibition

Authors and Affiliations

Sarah C. Atkinson [1,2], Con Dogovski [1,], Matthew T. Downton[3], Peter E. Czabotar[4], Renwick C.J. Dobson [2,5], Juliet A. Gerrard[5,6], John Wagner[3] and Matthew A. Perugini[1,2#]

[1]Department of Biochemistry, La Trobe Institute for Molecular Science, La Trobe University, Melbourne, Victoria 3086, Australia.

[2]Department of Biochemistry and Molecular Biology, Bio21 Molecular Science and Biotechnology Institute, 30 Flemington Road, The University of Melbourne, Victoria 3010, Australia,

[3]IBM Research Collaboratory for Life Sciences-Melbourne, Victorian Life Sciences Computation Initiative, Carlton, VIC 3010, Australia

[4]The Walter and Eliza Hall Institute of Medical Research, Parkville, 3052, Victoria, Australia

[5]Biomolecular Interaction Centre and School of Biological Sciences, University of Canterbury, Private Bag 4800, Christchurch, New Zealand

[6]Industrial Research Limited, PO Box 31310, Lower Hutt 5040, New Zealand

[#]Address correspondence to: A/Prof Matthew Anthony Perugini. Department of Biochemistry, La Trobe Institute for Molecular Science, La Trobe University, Melbourne, Victoria 3086, Australia. Tel: +61 3 9479 6570. Fax: +61 3 9479 1266; E-mail: M.Perugini@latrobe.edu.au

ABSTRACT

Lysine is one of the most limiting amino acids in plants and its biosynthesis is carefully regulated through inhibition of the first committed step in the pathway catalyzed by dihydrodipicolinate synthase (DHDPS). This is mediated via a feedback mechanism involving the binding of lysine to the allosteric cleft of DHDPS. However, the precise allosteric mechanism is yet to be defined. We present a thorough enzyme kinetic and thermodynamic analysis of lysine inhibition of DHDPS from the common grapevine, *Vitis vinifera* (*Vv*). Our studies demonstrate that lysine binding is both tight (relative to bacterial DHDPS orthologs) and cooperative. The crystal structure of the enzyme bound to lysine (2.4 Å) identifies the allosteric binding site and clearly shows a conformational change of several residues within the allosteric and active sites. Molecular dynamics (MD) simulations comparing the lysine-bound (PDB ID 4HNN) and lysine free (PDB ID 3TUU) structures show that Tyr132, a key catalytic site residue, undergoes significant rotational motion upon lysine binding. This suggests proton relay through the catalytic triad is attenuated in the presence of lysine. Our study reveals for the first time the structural mechanism for allosteric inhibition of DHDPS from the common grapevine.

Keywords: allostery; analytical ultracentrifugation; circular dichroism spectroscopy; dihydrodipicolinate synthase; enzyme; grapevine; lysine biosynthesis; molecular dynamics simulations; X-ray crystallography.

Abbreviations: ASA, (*S*)-aspartate semialdehyde; DHDPR, dihydrodipicolinate reductase; DHDPS, dihydrodipicolinate synthase; Pyr, pyruvate; lysine, (*S*)-lysine; threonine, (*S*)-threonine; *Vv*, *Vitis vinifera*.

INTRODUCTION

The grapevine (genus *Vitis*) is one of the world's most economically-important crops that in 2010 generated approximately $40 billion to the global economy (Nicholson et al. 2012). A significant proportion of the economic value of grapevine arises from wine production and sales with 4.4. billion litres of wine produced globally in 2010 (Nicholson, Tarlyn et al. 2012). Cultivars of the European wine grape (*Vitis vinifera*) form the basis of the majority of wines produced around the world, making it the most cultivated and economically important grape species (Vivier and Pretorius 2002). However, one of the most limiting nutrients in grape is the amino acid, lysine (Igartuburu et al. 1991; Nunan et al. 1997). Indeed, many crops contain low levels of lysine and therefore attempts have been made to increase the lysine content of agriculturally-important plants by classical breeding, mutant selection, or by genetic modification (van der Meer et al. 2001).

Of the enzymes that function in the lysine biosynthesis pathway, dihydrodipicolinate synthase (DHDPS) (Fig. 1) has attracted the most interest in lysine up-regulation (Zhu and Galili 2003). The enzyme is also as a promising target for antimicrobial discovery (Cox et al. 2000; Perugini et al 2005; Hutton et al. 2007; Boughton et al. 2008; Mitsakos et al, 2008; Dogovski 2009; Dogovski 2012). DHDPS catalyses the condensation of pyruvate and (*S*)-aspartate semialdehyde (ASA) to form (4*S*)-4-hydroxy-2,3,4,5-tetrahydro-(2*S*)-dipicolinic acid (HTPA) (Blickling, Renner et al. 1997). The DHDPS catalysed reaction is the first committed step of the lysine biosynthesis pathway (Fig. 2) (Hutton et al. 2007; Dogovski 2009; Atkinson et al. 2012; Dogovski 2012). The reaction proceeds via a ping-pong kinetic mechanism in which pyruvate binds and forms a Schiff base to an active-site lysine residue (Lys184 in *Vitis vinifera* DHDPS). ASA then reacts with the resultant enamine and following cyclization forms the product HTPA (Blickling, Renner et al. 1997). HTPA is then converted in several enzymatic steps to lysine (Fig. 2) (Hutton et al. 2007; Dogovski 2009; Dogovski 2012).

The structure of DHDPS has been studied extensively in a number of bacteria (Mirwaldt et al. 1995; Dobson, Griffin et al. 2005; Blagova et al. 2006; Burgess et al. 2008; Devenish et al. 2008; Dobson et al. 2008; Girish et al. 2008; Kefala et al. 2008; Voss et al. 2010). The bacterial form of the enzyme usually consists of a homotetramer of four identical $(\beta/\alpha)_8$-barrel monomers (Fig.

1a), with the active site situated near the center of the barrel. The tetramer can be described as a dimer of tight dimers, with two tight-dimers binding in a 'head-to-head' manner (Dobson, Griffin et al. 2005; Voss et al. 2010). By contrast, DHDPS enzymes from plants have been less extensively studied. The enzyme is encoded by the nuclear localized *dapA* gene and imported into plastids where DHDPS functions (Ghislain et al. 1990; Shaul and Galili 1992a; Vauterin and Jacobs 1994). We recently determined the crystal structure of DHDPS from *Vitis vinifera* (Atkinson, Dogovski et al. 2012), which, along with that of DHDPS from *Arabidopsis thaliana* (Griffin et al. 2012) and *Nicotiana sylvestris* (Blickling, Beisel et al. 1997) also forms a homotetramer, or dimer of tight dimers, but with an alternative architecture to that observed in bacteria referred to as a 'back-to-back' dimer-of-dimers (Fig. 1b).

The lysine biosynthetic pathway in plants is regulated by several feedback inhibition loops (Fig. 2). Aspartokinase, the first enzyme in the pathway, is feedback inhibited by lysine and threonine; whilst DHDPS is feedback inhibited by the final product of the pathway, lysine. Evidence suggests that DHDPS is the main regulatory point in higher plants, given that *Nicotiana sylvestris* mutants with lysine-desensitized DHDPS overproduces lysine (Frankard et al. 1992), whereas mutants that have aspartokinase desensitized to lysine inhibition overproduce threonine (Shaul and Galili 1992b).

The negative feedback inhibition of DHDPS by lysine has been investigated in several Gram-negative bacteria, Gram-positive bacteria, and also plant species. DHDPS from Gram-negative bacteria such as *Escherichia coli* (Yugari and Gilvarg 1965; Soares da Costa et al. 2010) and *Neisseria meningitidis* (Devenish et al. 2009) are weakly inhibited with IC_{50} values ranging from 0.25 mM to 1.0 mM. Whereas, DHDPS from Gram-positive bacteria such as *Bacillus lichenformis* (Halling and Stahly 1976), *Bacillus megaterium* (Webster and Lechowich 1970), *Bacillus subtilis* (Yamakura et al. 1974), *Bacillus anthracis* (Blagova, Levdikov et al. 2006; Domigan et al. 2009; Voss et al. 2010), *Corynebacterium glutamicum* (Cremer et al. 1988), *Bacillus cereus* (Hoganson and Stahly 1975), *Lactobacillus plantarum* (Cahyanto et al. 2006) and methicillin-resistant *Staphylococcus aureus* (MRSA) (Burgess et al. 2008) show no inhibition by lysine, including concentrations higher than is considered physiologically relevant (up to 50 mM). By contrast, DHDPS from the plant species *Triticum aestivum* (Kumpaisal et al.

1987), *Daucus carota sativa* (Matthews and Widholm 1979), *Spinacia oleracea* (Wallsgrove and Mazelis 1980), *Zea mays* (Frisch et al. 1991) and *Pisum sativum* (Dereppe et al. 1992) are strongly inhibited by lysine with IC_{50} = 10-50 µM. It is therefore not surprising that lysine is one of the most limiting amino acids in plants.

Accordingly, a range of transgenic plants have been developed in which DHDPS has been genetically manipulated with the aim of producing high-lysine crops (Frankard et al. 1992; Perl et al. 1992; Shaul and Galili 1992a; Galili 1995; Ghislain et al. 1995; Kwon et al. 1995; Bittel et al. 1996; Brinch-Pedersen et al. 1996; Silk and Matthews 1997). The introduction of feedback-insensitive DHDPS enzymes that lack the propensity to bind lysine allosterically resulted in a 10- to 100-fold overproduction of lysine (Negrutiu et al. 1984; Frankard et al. 1992; Shaul and Galili 1993; Ben-Tzvi Tzchori et al. 1996; Sarrobert et al. 2000). This demonstrates that removal of lysine-mediated allosteric inhibition greatly influences the lysine content of plants.

Kinetic and structural studies show that lysine is an allosteric inhibitor causing partial inhibition (90%) at saturating concentrations (Yugari and Gilvarg 1965). The structure of *E. coli* DHDPS co-crystallized with lysine (PDB ID: 1YXD) revealed two lysine molecules bind the allosteric site in a back-to-back orientation with the alpha carbon of each lysine separated by 4.10 Å (Dobson, Griffin et al. 2005). Isothermal titration microcalorimetry (ITC) experiments show that inhibition is cooperative with the second molecule of lysine binding 10^5 times more tightly than the first (Phenix and Palmer 2008; Muscroft-Taylor et al. 2010). In addition, a structural study of DHDPS from the plant *N. sylvestris* suggests a conformational change occurs upon lysine binding (Blickling, Beisel et al. 1997). Several of the residues involved in contacts at the tight dimer interface are displaced when lysine is bound, dislocating the dimers in relation to each other. However, this altered conformation was not observed in the *E. coli* DHDPS structure bound to lysine (Dobson, Griffin et al. 2005). Therefore, the precise mechanism of lysine-mediated allosteric inhibition of DHDPS remains elusive.

Here, we present thorough kinetic and thermodynamic analyses of lysine-mediated allosteric inhibition in DHDPS from *Vitis vinifera* (*Vv*-DHDPS). We also describe the crystal structure of the enzyme bound to lysine (2.4 Å); and subsequently employ molecular dynamics (MD)

simulations comparing the structures of *Vv*-DHDPS in the absence (PDB ID 3TUU) and presence of lysine (PDB ID 4HNN). These structural and computational studies reveal a significant rotation of Tyr132 suggesting binding of lysine attenuates the function of this catalytic triad residue. Our results offer significant insight into the allosteric regulation of an important plant enzyme.

MATERIALS AND METHODS

Cloning, Expression and Purification of *Vv*-DHDPS

The *dapA* gene encoding DHDPS from *Vitis vinifera* was purchased from Geneart and cloned into the pET28a expression vector as described elsewhere (Atkinson et al. 2011). Recombinant protein was produced in the host strain *E. coli* BL21-DE3 via induction by IPTG at 16 °C as described previously (Atkinson et al. 2011). Briefly, cells were harvested after an overnight induction (1 mM IPTG) and resuspended in 20 m*M* Tris-HCl, pH 8.0, 500m*M* NaCl, 20 m*M* imidazole prior to lysis by sonication. *Vv*-DHDPS was subsequently isolated by metal-affinity liquid chromatography as described elsewhere (Atkinson et al. 2011).

DHDPS-DHDPR Coupled Enzyme Kinetic Assay

Kinetic analyses of *Vv*-DHDPS were performed using the DHDPS-DHDPR coupled assay as described elsewhere (Dobson et al. 2004), using *E. coli* DHDPR as the coupling enzyme. Assays were routinely performed in triplicate at a constant temperature of 30 °C with reaction mixtures allowed to equilibrate in a temperature-controlled Cary 4000 UV-visible spectrophotometer for 10 min before initiating the reaction with 60 n*M* DHDPS. Prior to conducting kinetic measurements, pyruvate and ASA concentrations were quantified by the addition of limiting amounts of substrate and measuring the oxidation of NADPH spectrophotometrically at 340 nm. Initial rate data were analyzed using the ENZFITTER program available from Biosoft. Data were fitted to appropriate models as judged by Sigma values and the lowest standard error associated with the kinetic constants. Initial velocity data were fitted to the ping-pong model (1), mixed inhibition model (2), or non-competitive inhibition model (3), where appropriate, using the following kinetic equations:

$$v = V\,AB / (K_{mB}A + K_{mA}B + AB) \quad (1)$$

$$v = VA/(\{K_m^{app}(1 + (I/K_i)^{n}_{ES})\} + \{A(1 + (I/K_i')^{n}_{E})\}) \quad (2)$$

$$v = VA/\{(1 + (I/K_i)^{n}_{ES})\,(K_m^{app} + A)\} \quad (3)$$

Here V is the maximal velocity, A and B are the substrate concentrations, K_{MA} and K_{MB} are the Michaelis–Menten constants for each substrate, and v is the initial velocity. K_M^{app} is the apparent Michaelis–Menten constant in models (2) and (3), while K_i and K_i are the inhibition constants for I binding to the ES and E complex, respectively. n_{ES} and n_E are the Hill coefficient for I binding to the ES and E complex, respectively.

Hill equation (Hill, 1910):
$\log(v/V\text{-}v) = -\log(I) - \log K_d$

Isothermal Titration Microcalorimetry

Calorimetric experiments were conducted using an ITC instrument (VP-ITC, MicroCal Inc, Northampton, MA, USA) using methods based on those outlined by Turnbull and Daranas (Turnbull and Daranas 2003). Prior to ITC experiments, protein samples were exchanged into ITC buffer (200 m*M* HEPES, 5m*M* pyruvate, pH 7.7) by overnight dialysis. A portion of the buffer was retained for flushing the instrument, blank measurements, and preparation of solutions containing ligand. All experiments were conducted at 20 °C and solutions were degassed under vacuum prior to use. A typical 35-injection protocol employed titrating ligand into *Vv*-DHDPS (initial concentration of 80 μ*M*) protein solution using the following parameters: 1 × 10 μL, then 34 × 12 μL at 180 s intervals, using a syringe rotating at 310 rpm. The concentrations of ligands used were 2.5 and 10 m*M* lysine which was made up in the stock ITC buffer solution. Heats of dilution determined in the absence of protein were subtracted from the titration data prior to curve fitting. Additionally, the initial 10 μL injection was discarded from each dataset in order to remove the effect of titrant diffusion across the syringe tip during the equilibration process. Curve fitting was undertaken in Origin version 7.0 (OriginLab Corporation, Northampton, MA, USA) using the fitting algorithms supplied by MicroCal.

CD Spectroscopy

Circular dichroism (CD) spectra of *Vv*-DHDPS (4 µ*M*) were recorded using an Aviv Model 410-SF CD spectrometer. Wavelength scans were performed between 198 and 250 nm in 20 m*M* Tris, 150 m*M* NaCl, pH 8.0 in 1.0 mm quartz cuvette as reported previously (Davis et al. 2004; Burgess et al. 2008; Voss et al. 2010). Data were analysed using the CDSSTR algorithm from the CDPro software package (Sreerama and Woody 2000; Davis et al. 2004) incorporating the SP22X protein database. For thermal denaturation scans, ellipticity at 222 nm was monitored between 20 and 90 °C in 1 °C steps

Analytical Ultracentrifugation

Sedimentation velocity experiments were performed in a Beckman Coulter model XL-I analytical ultracentrifuge using similar methods to that reported previously (Atkinson et al 2012; Burgess et al 2008; Perugini et al. 2000; Voss et al 2010). Double sector quartz cells were loaded with 400 µL of buffer and 380 µl of *Vv*-DHDPS at an initial concentration of 13 µ*M*. The cells were loaded into an An50-Ti rotor and left to equilibrate at 30 °C. A rotor speed of 40,000 rpm was employed and absorbance readings were collected continuously at 280 nm (30 °C) using a step size of 0.003 cm without averaging. Initial scans were carried out at 3,000 rpm to determine the optimal wavelength and radial positions for the high speed experiment. Samples of *Vv*-DHDPS monitored in the presence of 1.0 m*M* lysine contained ligand in both the reference and sample channels. Solvent density, solvent viscosity, and estimates of the partial specific volume of *Vv*-DHDPS (0.7386 ml/g) at 30 °C were calculated using SEDNTERP (Laue 1992). Data were analyzed via the ULTRASCAN software package (Demeler and van Holde 2004; Demeler 2005a; Demeler 2005b), which can be downloaded from www.ultrascan.uthscsa.edu.

Crystallization of *Vv*-DHDPS and X-ray Diffraction Data

Initial crystallization trials were performed as previously described (Atkinson et al. 2011) using droplets consisting of 150 nl protein solution (in the presence of 20 mM pyruvate and 20 mM lysine) and 150 nL reservoir solution. Initial hit conditions were up scaled using the hanging-drop vapor-diffusion method with drops consisting of protein solution (2 µL) and precipitant solution (2 µL) at 293 K. As noted with crystals grown in the presence of pyruvate alone

(Atkinson et al. 2011), crystal growth in the presence of pyruvate and lysine required the precipitant concentration to be halved and protein concentration reduced to 2.5 mg/ml. A variety of crystal forms were observed from a number of different conditions. The best diffracting crystal (Supplementary Figs. 6a & 6b) grew from a modified version of condition 22 (0.1 *M* MES pH 6.5, 6% (v/v) PEG 20,000), Hampton Research Crystal Screen 2. For X-ray data collection, a single crystal was transferred to a reservoir solution containing 20% (v/v) glycerol and directly flash frozen in liquid nitrogen. Intensity data were collected at 110 K at the Australian Synchrotron on the MX2 beamline (Evans and Pettifer 2001; McPhillips et al. 2002) using X-rays with a wavelength of 0.9536 nm. Data was collected in 0.5° steps with an exposure time of 2 s for one 360° pass, using an ADSC Q310r CCD detector positioned 280 mm from the crystal. Diffraction data sets were processed and scaled using the package MOSFLM (Leslie 2007) and SCALA (Collaborative Computational Project 1994; Evans 2006). Molecular replacement was performed using PHASER (McCoy et al. 2007) with pyruvate-bound *Vv*-DHDPS (PDB ID: 3TUU (Atkinson et al. 2012)) as the search model. Structural refinement of the resulting eight monomers in the asymmetric unit was performed using REFMAC5 (Collaborative Computational Project 1994; Murshudov et al. 1997) with iterative model building using COOT (Emsley and Cowtan 2004). In the first steps of refinement, non-crystallographic restraints were applied, followed by simulated annealing using PHENIX (Adams et al. 2010). The structure was validated using the MolProbity Server (Chen et al. 2010). Refinement statistics are presented in Table 3. Ramachandran statistics showed 98.2% of the residues in the most favored region, 1.5% in the additionally allowed regions and 0.5% (a single residue) in the disallowed region, namely Tyr 132, which is consistent with the equivalent Tyr residues observed in DHDPS structures from other species (Dobson, Griffin et al. 2005; Blagova et al. 2006).

Molecular Dynamics Simulations

Two independent molecular dynamics simulations were performed using tetrameric structures of *Vv*-DHDPS in the presence (PDB ID: 4HNN) and absence (PDB ID: 3TUU) of lysine. Residues outside the range 21-327 were removed from starting structures and the substrate, pyruvate, was removed from Lys184. Structures were solvated using the TIP3P water model in a rhombic dodecahedral shaped periodic box. The net charge of the simulation box was set to zero through

the addition of sodium ions and additional ions were added to give an ionic concentration of 150 m*M* NaCl. The CHARMM force field (MacKerell et al. 1998) and the molecular dynamics package NAMD (Phillips et al. 2005) were used. Trajectories of 150 ns were generated at a constant temperature of 293K and atmospheric pressure. Snapshots of the full system were taken at 0.01 ns intervals and stored for analysis using VMD (Humphrey et al. 1996). Clustering of results was performed on a concatenated trajectory that contained a tight dimer pair from both the simulations. The clustering tool available in VMD was used with an RMSD based cutoff.

RESULTS AND DISCUSSION

Vv-DHDPS is Tightly Inhibited by Lysine

To characterize the kinetic properties of *Vv*-DHDPS, the coupled enzyme assay utilizing *E. coli* dihydrodipicolinate reductase (DHDPR, Fig. 2) as the coupling enzyme (Dobson et al. 2004) was performed at varying lysine and substrate (i.e. pyruvate and ASA) concentrations. Fig. 3a shows plots of initial velocity as a function of lysine and pyruvate concentrations. The plots reveal a sigmoidal relationship that is characteristic of cooperative allosteric enzyme inhibition (Cornish-Bowden 1976). The equivalent kinetics data determined at varying ASA concentrations are plotted in Supplementary Fig. 1a. Subsequent Hill plots were generated to provide estimates of the Hill coefficient (n_{app}). This yielded n_{app} of 1.9 with respect to pyruvate (Fig. 3b) and 1.7 with respect to ASA (Supplementary Fig. 1b). The data indicates positive cooperativity and suggests that the binding of one lysine molecule increases the affinity of the enzyme for additional molecules (Cornish-Bowden 1976).

The mode of lysine inhibition with respect to both substrates was next investigated. The effect of increasing lysine concentrations at either (i) fixed pyruvate concentration (5 mM) and varied ASA concentrations or (ii) fixed ASA (1.2 mM) and varied pyruvate concentrations was examined. In both cases, the double reciprocal plots (Supplementary Fig. 2) intersected to the left of the 1/V axis indicating both K_M and V_{max} are affected by the presence of lysine. This is characteristic of mixed inhibition, indicating that lysine binds to free DHDPS and also the DHDPS-substrate complex (Supplementary Fig. 2). Fitting the data to a mixed inhibition model revealed $K_{i(ES)}$= 0.063 mM and $K_{i(E)}$= 0.054 mM with respect to pyruvate, suggesting a slightly

lower affinity for the DHDPS-pyruvate complex compared to the free enzyme (Fig. 3a, Table 1).The resulting Hill coefficients were 1.0- and 2.4 for n_{ES} and n_E, respectively (Table 1).. With respect to ASA, lysine is a noncompetitive inhibitor (affinity for E and ES is the same) with a single K_i of 0.049 mM and n_E of 1.7 (Supplementary Fig. 1a, Table 1). K_i values for lysine of less than 0.1 mM are consistent with that observed for DHDPS from the other plant species, including *T. aestivum* (Kumpaisal et al. 1987), *D. carota sativa* (Matthews and Widholm 1979), *S. oleracea* (Wallsgrove and Mazelis 1980), *Z. mays* (Frisch et al. 1991) *and P. sativum* (Dereppe et al. 1992) and are significantly tighter than those typically observed for DHDPS from Gram-negative bacteria (Yugari and Gilvarg 1965; Devenish et al. 2009; Soares da Costa et al. 2010).

To verify the cooperativity observed in the enzyme kinetic data and determine accurate lysine binding affinities at equilibrium, the thermodynamics of lysine binding to *Vv*-DHDPS was measured by isothermal titration microcalorimetry (ITC) in the presence of saturating pyruvate. Titration of 80 μM *Vv*-DHDPS with 10 mM lysine (Supplementary Fig. 3a) and 2.5 mM lysine (Supplementary Fig. 3b) generated isotherms diagnostic of cooperative binding, in which ligand addition initially results in increasing heat of association, followed by binding site saturation (Bradrick et al. 1996; Phenix and Palmer 2008). As the two lysine molecules occupy symmetry-related binding sites within the allosteric cleft, the binding isotherm was fitted to a sequential binding site model, as described previously (Muscroft-Taylor et al. 2010). The resulting thermodynamic parameters are presented in Table 2. Interaction of the first lysine (Lys_1) with the binding site was characterized by an affinity of 2 μM comprised primarily of an entropic effect with a small enthalpic contribution (Table 2). By contrast, the second binding interaction (Lys_2) is 190-fold weaker in affinity, but has a significantly greater enthalpic contribution with a reduced entropic component (Table 2). This appears to be a case of enthalpy-driven positive cooperativity (Ricard & Cornish-Bpwden, 1987), which is consistent with previous ITC studies of *E. coli* DHDPS titrated with lysine (Muscroft –Taylor et al 2010). However, the affinities of *Vv*-DHDPS for lysine are significantly tighter than the *E. coli* enzyme. In contrast, ITC studies show that the binding energy of MosA for lysine was characterized as primarily entropic for both sites, in which the second site contributed >90% of the interaction energy (Phenix and Palmer 2008).

Pyruvate and Lysine Significantly Stabilize the Secondary Structure of *Vv*-DHDPS

Recent studies show that the thermostability of bacterial DHDPS enzymes is significantly enhanced in the presence of pyruvate, which is the first substrate to bind the enzyme (Burgess et al. 2008; Domigan et al. 2009; Voss et al. 2010). However, no change in thermostability is observed in the presence of ASA, the second substrate to bind in the DHDPS-catalysed reaction (Burgess et al. 2008; Voss et al. 2010). By contrast, the effect of lysine on the thermostability of plant DHDPS has not yet been reported. To assess if lysine influences the thermostability of *Vv*-DHDPS in solution, circular dichroism (CD) spectroscopy studies were conducted. Initially, wavelength scans were measured at 20 °C to compare the global secondary structure of *Vv*-DHDPS in the absence and presence of ligand. This revealed no significant change in secondary structure upon addition of saturating amounts of pyruvate or lysine (Supplementary Fig. 4). Thermal denaturation experiments were subsequently performed in the presence and absence of saturating concentrations of ligands over the temperature range of 20–90 °C (Fig. 4a). *Vv*-DHDPS appears to follow a two-state mechanism for thermal unfolding in the absence of ligands, with an apparent melting temperature of 59.0°C (Fig. 4a). However, in the presence of 5.0 mM pyruvate or 1.0 mM lysine, the thermal denaturation of *Vv*-DHDPS is delayed with respect to temperature, with apparent melting temperature increasing significantly to 67.1 °C and 64.7 °C, respectively. Interestingly, the presence of both ligands markedly accentuates the thermostability of the enzyme with the apparent melting temperature increasing to 73.0°C (Fig. 4a). Although no secondary structural changes were observed in the presence of ligands, the significant increase in thermostability in the presence of pyruvate and/or lysine may be associated with changes in tertiary and/or quaternary structure. Indeed, pyruvate has previously been shown to stabilize the quaternary structure of bacterial DHDPS enzymes (Burgess et al. 2008; Voss et al. 2010), but to date, there have been no studies demonstrating the effect of lysine on the quaternary structure of DHDPS.

Lysine Does Not Change the Quaternary Structure of *Vv*-DHDPS in Solution

To determine if lysine influences the quaternary structure of *Vv*-DHDPS, sedimentation velocity experiments were conducted in the analytical ultracentrifuge. Interestingly, recent studies show that dimeric mutants of bacterial DHDPS possess significantly attenuated catalytic function compared to their wild-type tetrameric counterparts (Griffin et al. 2008; Griffin et al. 2010; Voss

et al. 2010). It is thus possible, that lysine mediates allosteric inhibition by inducing dissociation of the *Vv*-DHDPS tetramer (Fig. 1b) into less active dimers that are nonetheless more thermostable. However, in both the absence and presence of lysine, the absorbance versus radial position profiles of *Vv*-DHDPS show a single sedimenting boundary whose rate of movement appears unchanged upon addition of ligand suggesting there is no change in quaternary structure (Supplementary Fig. 5). This assertion is supported by analyzing the data in a model-independent manner using the enhanced van Holde-Weischet method employing the ULTRASCAN software suite (Demeler and van Holde 2004; Demeler 2005a; Demeler 2005b). As shown in Fig. 4b, the resultant distributions show that *Vv*-DHDPS in the presence or absence of lysine exists as a single 7.2 S species, which correlates to the tetrameric form (Fig. 1b) (Atkinson et al. 2012). This verified that the quaternary structure of *Vv*-DHDPS remains unchanged in the presence of lysine, suggesting that lysine-enhanced thermostability is mediated through changes in tertiary structure.

Structure of *Vv*-DHDPS in Complex with Lysine Reveals a Conformational Change

Given that lysine enhances enzyme thermostability but does not alter the secondary or quaternary structure of *Vv*-DHDPS, we next set out to examine the tertiary structural changes, if any, accompanying binding of the allosteric inhibitor. As described previously (Atkinson et al. 2011), attempts to crystallize *Vv*-DHDPS in the absence of ligand were unsuccessful, but the addition of pyruvate resulted in crystal formation, although in-drop thrombin cleavage was required to generate diffracting crystals. Crystal trials in the presence of both pyruvate and lysine were much more successful, with several conditions producing large crystals without the need for in-drop thrombin cleavage. The best diffracting crystal (Supplementary Figs. 6a & 6b) was cultivated from a modified version of condition 22 of Hampton Research Crystal Screen 2 (reservoir solution: 0.1M MES pH 6.5, 6% (v/v) PEG 20,000). This result correlates with solution-based studies of *Vv*-DHDPS described above, where the addition of both pyruvate and lysine significantly increase the thermostability of the enzyme (Fig. 4a).

The crystal structure of *Vv*-DHDPS in the presence of pyruvate & lysine was determined by molecular replacement using pyruvate-bound *Vv*-DHDPS (PDB ID 3TUU) as the search model (Fig. 1b). The structure (PDB ID 4HNN) revealed two tetramers of *Vv*-DHDPS in the asymmetric unit, both displaying a ‘back to back’ quaternary architecture (Fig. 5a) as previously

observed for DHDPS from *N. sylvestris* (Blickling, Beisel et al. 1997), *A. thaliana* (Griffin et al. 2012) and the pyruvate-bound structure from *V. vinifera* (Atkinson et al. 2012) (Fig. 1b). The r.m.s.d. between the two tetramers is 2.9 Å. The final molecule had an overall R_{cryst} of 18.4% (R_{free} of 22.0%) to 2.4 Å resolution. The 4HNN model was also examined using the MolProbity server (Chen et al. 2010), which revealed that 98.2% of residues in *Vv*-DHDPS bound to lysine and pyruvate were located in the favored regions of the Ramachandran plot. The eight residues in the 'disallowed' regions correspond to the catalytic site residue Tyr132 from each of the eight chains. This is not unexpected as this highly conserved residue has been shown to reside in the disallowed region of the Ramachandran plot in all other DHDPS structures determined to date (Mirwaldt et al. 1995; Dobson, Griffin et al. 2005; Blagova et al. 2006; Burgess et al. 2008; Devenish et al. 2008; Dobson et al. 2008; Girish et al. 2008; Kefala et al. 2008; Voss et al. 2010; Atkinson et al. 2012). A summary of the crystallographic data collection and refinement statistics is provided in Table 3.

The structure shows that each monomer is comprised of an N-terminal $(\beta/\alpha)_8$-barrel domain and a C-terminal domain consisting of 3 α-helices and 2 short β-strands (Supplementary Fig. 7a). As for the pyruvate-bound structure (PDB ID 3TUU) (Atkinson et al. 2012), the N terminus of each monomer is absent from the observed electron density, presumed to be mostly disordered. Owing to the crystallization conditions used, electron density associated with pyruvate is found covalently bound to the active site lysine (Lys184) in each subunit. The active site forms around this key lysine residue, which is located at the center of each monomeric unit (Supplementary Fig. 7b). The spatial orientation of the three conserved catalytic triad residues, namely Tyr132, Thr69 and Tyr156, as well as Arg161 and Ile223 that are also important for catalytic activity, is consistent with that observed in the active sites of other DHDPS structures (Dobson, Devenish et al. 2005; Dobson et al. 2008; Dobson et al. 2004)

Following the first round of refinement, electron density was observed at the tight dimer interfaces of both tetramers, which was not accounted for by the search model (PDB ID 3TUU). Subsequent manual modeling of this density supports the occupancy of two lysine molecules bound in the allosteric pocket at the interface of the tight dimer (i.e. interface ab or cd, Fig. 5a) and in weak contact with each other (3.5 Å between alpha carbons) (Fig. 5b). Following final

refinement, an omit map was generated, confirming the presence and orientation of the lysine molecules (Supplementary Fig. 8). The refined structure shows that the carboxyl group of lysine is coordinated by the hydroxyl group of Tyr131 and the amide of the Asn105 of the adjacent subunit. Importantly, the α-amino group forms a salt bridge with Glu109 and a hydrogen bond with Asn105, as well as a hydrogen bond with Gln74 (Fig. 5b). Since crystals were generated at pH 6.5, the amino group of lysine would be in a protonated state and thus able to form a salt bridge. The ε-amino group is coordinated by Trp78, His81 and a hydrogen bond with the main-chain oxygen atom of Gly73 (Fig. 5b). Additional van der Waals contacts are formed with Met76, Ser77, Asn101, Gly103, Ser104, Ser106 and Tyr132, completing the allosteric site.

As stated earlier, a range of transgenic plants have been generated in which point-mutations targeting DHDPS have abolished lysine inhibition (Frankard et al. 1992; Perl et al. 1992; Shaul and Galili 1992a; Galili 1995; Ghislain et al. 1995; Kwon et al. 1995; Bittel et al. 1996; Brinch-Pedersen et al. 1996; Silk and Matthews 1997). For instance, Trp78Arg (Vauterin et al. 2000), Asn105Ile (Ghislain et al. 1995), Ser104Asn (Shaver et al. 1996) and Glu109Lys (Shaver et al. 1996) (*Vv*-DHDPS numbering) substitutions in DHDPS from a number of plant species have resulted enzymes that are not regulated by lysine. Our study of *Vv*-DHDPS shows that these residues are important for stabilizing allosteric interactions. Interestingly, an Ala113Val substitution (Bittel et al. 1996; Shaver et al. 1996; Silk and Matthews 1997) has also resulted in lysine-insensitivity. The reason for this is at first unclear, given that Ala113 does not appear to make contacts with lysine bound in the allosteric cleft. However, close inspection of the allosteric site reveals the close proximity of Ala113 to Trp78, and thus it is likely that a valine substitution displaces Trp78 interfering with lysine binding.

Both the pyruvate & lysine bound (Fig. 5a) and the previously reported pyruvate-bound (Fig. 1b) (Atkinson et al. 2012) structures of *Vv*-DHDPS are very similar. The backbone of the two tetramers align with an r.m.s.d. of 0.34 Å with no significant differences observed in the key active site residues (Supplementary Fig. 7b). However, it is noted that Trp78 in the allosteric cleft moves significantly upon lysine binding (Fig. 6a, Supplementary Fig 9a). This residue acts as a lid, greatly reducing the solvent accessibility of the allosteric site once lysine is bound (Figs. 6b & 6c). This movement, together with a rearrangement of residues H81 (Supplementary Fig.

9b) and I82, is similar to that seen in *N. sylvestris* DHDPS (Blickling, Beisel et al. 1997). Notably, however, the small displacement of helix α2 towards the inhibitor binding pocket observed in *N. sylvestris* DHDPS upon lysine binding (Blickling, Biesel et al. 1997) is not apparent in *Vv*-DHDPS. Likewise, rearrangement of the tight-dimer units in *N. sylvestris* DHDPS upon lysine binding (Blickling, Biesel et al. 1997) is not observed for the *Vv*-DHDPS structure reported in this study.

Following lysine binding to *Vv*-DHDPS, the hydroxyl group of Tyr131 is drawn towards the carboxyl group of lysine, changing its position by 0.69 ± 0.09 Å averaged across 8 monomers in the asymmetric unit (Supplementary Fig. 9c). Tyr131 forms a hydrophobic stack with the interdigitating catalytic triad residue, Tyr132, which is contributed by the adjacent monomer across the tight dimer interface (Supplementary Fig. 7b). The reorientation of Tyr131 upon lysine binding disrupts this packing, displacing the hydroxyl group of Tyr132 by 0.56 ± 0.05 Å (Supplementary Fig. 9c). We propose this is sufficient to disrupt the function of the catalytic triad, which involves proton relay from pyruvate through the catalytic triad of Tyr156-Thr69-Tyr132 to solvent (Supplementary Fig. 7b) (Dobson et al., 2004). This suggests a potential structural mechanism for lysine-mediated allosteric inhibition through the abrogation of catalytic triad function.

In addition to elucidating significant differences in the orientation of key allosteric and active site residues, it was anticipated that the structure of *Vv*-DHDPS bound to lysine would also provide insight into the enhanced thermostability observed for the enzyme in the presence of lysine (Fig. 4a). Computational analyses using the Protein Interfaces, Surfaces and Assemblies (PISA) program available on the European Bioinformatics Institute website (Krissinel and Henrick 2007) show that the total solvent inaccessible surface area (SISA) at the 'tight' dimer interface of lysine-bound *Vv*-DHDPS is 1827 $Å^2$ compared to 1788 $Å^2$ at the equivalent interface of the *Vv*-DHDPS structure in the absence of lysine (Supplementary Table 1). The larger buried surface area is due to a greater number of residues comprising this interface. Of note, two additional residues contribute to hydrogen bond formation, whilst one additional residue contributes to an ion-ion interaction across this interface (Supplementary Table 1). Together, the increase in SISA and additional contacts would explain the increased stability observed in thermal denaturation

studies (Fig. 4a). By contrast, minor differences exist between the two structures at the weak dimer interface with a slight reduction in SISA, but a subtle increase in the total number of noncovalent interactions upon lysine binding (Supplementary Table 1).

Comparison of Plant and Bacteria Allosteric Sites

It has been observed that the K_i for lysine inhibition in plant DHDPS is often up to 20-fold tighter than that observed in bacterial DHDPS enzymes (Yugari and Gilvarg 1965; Webster and Lechowich 1970; Yamakura et al. 1974; Hoganson and Stahly 1975; Halling and Stahly 1976; Matthews and Widholm 1979; Kumpaisal et al. 1987; Cremer et al. 1988; Frankard et al. 1992; Shaul and Galili 1992b; Cahyanto et al. 2006; Burgess et al. 2008; Devenish et al. 2009; Domigan et al. 2009; Soares da Costa et al. 2010). To better understand the nature of this difference, the allosteric site of *Vv*-DHDPS was compared to the equivalent site in the structure of *E. coli* DHDPS bound to lysine (PDB ID: 1YXD) (Dobson, Griffin et al. 2005) (Supplementary Fig. 10). Many residues that make up the allosteric site of *E. coli* DHDPS (Dobson, Griffin et al. 2005) are conserved in *Vv*-DHDPS, including Asn105, Glu109 and His81 (*Vv*-DHDPS numbering). However, the plant binding cleft is narrower than the equivalent site in bacteria with the distance between adjacent lysine molecules spanning 3.5 Å in *Vv*-DHDPS compared to 4.1 Å in *E. coli* DHDPS. Most importantly, bacterial DHDPS enzymes lack an equivalent Trp78 residue. Instead, a histidine residue acts like a 'lid' upon lysine binding in the *E. coli* structure (Supplementary Fig. 10). This histidine residue lacks the steric bulk of a tryptophan, thus leaving the allosteric site much more exposed to solvent. In addition, whilst the allosteric site is located on the external surface of the molecule in *E. coli* DHDPS (Fig. 1a), the architecture of *Vv*-DHDPS means that the lysine binding site is located in the center of the tetramer in proximity to the adjacent dimer (Fig. 5a).

Molecular Dynamics Simulations

To provide further insight into the mechanism of lysine-mediated allosteric inhibition, molecular dynamics (MD) simulations were performed on lysine-bound *Vv*-DHDPS (PDB ID: 4HNN) compared to the lysine free enzyme (PDB ID: 3TUU). Fig. 7 summarizes the MD simulation results. The root mean squared deviation of the tetramer (Fig. 7a) shows that the lysine bound form (red trajectory) is tighter than the unoccupied form (black trajectory) with a lower deviation

from the crystal structure over the course of the 150 ns simulation. This is consistent with thermostability measurements in solution (Fig. 4a). The root mean squared fluctuation taken on a chain-by-chain basis shows a mixture of different fluctuations with no clear consensus that is dependent on the presence of lysine (Fig. 7a). However, changes in the dynamics of the catalytic triad can be observed particularly in the rotation of Tyr132 around the χ_2 dihedral angle (Fig. 7c). Although the crystal structure shows this key catalytic residue is displaced by 0.6 Å upon lysine binding (Supplementary Fig. 9c), MD simulations demonstrate lysine binding has a much more profound effect on the orientation and dynamics Tyr132. Analyses show that transitions between the equivalent orientations for Tyr132 happen infrequently during the 150 ns simulations for the unoccupied enzyme (Fig. 7c, upper panel), but relatively rapidly when lysine is bound to the allosteric site (Fig. 7c, lower panel). In addition, clustering of a mixed trajectory formed by concatenating tight-dimer trajectories from the lysine bound and lysine free simulations were performed (Fig. 7d). The clustering is based on the backbone conformation alone, but the two most occupied clusters discriminate between those structures that contain lysine in the allosteric site and those that do not, as seen by the orientation of Trp78 (Fig. 7d). These clusters contain quite different side chain orientations of key active and allosteric site residues, including Tyr132, when lysine is bound to the allosteric cleft. Overall, the MD simulation results show marked differences in the dynamics of key residues, particularly Tyr132, based on the occupancy of the lysine binding pocket. This supports the notion that the structural mechanism of lysine allosteric inhibition is mediated through enhanced dynamics and displacement of Tyr132, which results in inefficient catalytic triad function. Furthermore, this phenomenon explains why lysine is a partial inhibitor of DHDPS, since functional orientation of Tyr132 is still possible, but less likely in the presence of allosteric inhibitor.

Conclusions

In conclusion, we show using enzyme kinetic and calorimetric studies in solution that dihydrodipicolinate synthase (DHDPS) from *Vitis vinifera* is allosterically inhibited by lysine in a cooperative manner with 10-fold greater potency than that reported for bacterial orthologs. Although no change in secondary or quaternary structure is observed upon lysine binding, the allosteric inhibitor induces a significant increase in thermostability. This is manifested by conformational changes in key allosteric and active site residues, including Trp78, Tyr131 and

Tyr132. MD simulations provide further insight showing that lysine binding leads to enhanced rotation of Tyr132, which we propose abrogates the function of the catalytic triad of Thr69, Tyr156 and Tyr132. Together, these findings provide valuable structural insights into the mechanism of lysine-mediated allosteric inhibition of DHDPS from an agriculturally-important plant species.

ACKNOWLEDGEMENTS

We would firstly like to acknowledge the support and assistance of the friendly staff at the Bio21 Collaborative Crystallographic Centre at CSIRO Molecular and Health Technologies, Parkville, Melbourne and the beamline scientists at the Australian Synchrotron, Victoria, Australia. We would also like to thank all members of the Perugini laboratory for helpful discussions during the preparation of this manuscript. Finally, we acknowledge the Australian Research Council for providing a Future Fellowship for M.A.P. and P.C and the University of Melbourne (FRGSS 2011 Project grant) for project funding. R.C.J.D. acknowledges the CR Roper Bequest for Fellowship support. This research was supported by a Victorian Life Sciences Computation Initiative (VLSCI) grant number VR0089 on its Peak Computing Facility at the University of Melbourne, an initiative of the Victorian Government, Australia.

REFERENCES

Adams PD, Afonine PV, Bunkoczi G, Chen VB, Davis IW, Echols N, Headd JJ, Hung LW, Kapral GJ, Grosse-Kunstleve RW, McCoy AJ, Moriarty NW, Oeffner R, Read RJ, Richardson DC, Richardson JS, Terwilliger TC and Zwart PH (2010) PHENIX: a comprehensive Python-based system for macromolecular structure solution. Acta Crystallogr D Biol Crystallogr 66: 213-221.

Atkinson SC, Dogovski C, Downton MT, Pearce FG, Reboul CF, Buckle AM, Gerrard JA, Dobson RCJ, Wagner J and Perugini MA (2012) Crystal, solution and in silico structural studies of dihydrodipicolinate synthase from the common grapevine. PLoS One 7: e38318.

Atkinson SC, Dogovski C, Newman J, Dobson RC and Perugini MA (2011) Cloning, expression,

purification and crystallization of dihydrodipicolinate synthase from the grapevine *Vitis vinifera*. Acta Crystallogr Sect F Struct Biol Cryst Commun 67: 1537-1541.

Ben-Tzvi Tzchori I, Perl A and Galili G (1996) Lysine and threonine metabolism are subject to complex patterns of regulation in *Arabidopsis*. Plant Mol Biol 32: 727-734.

Bittel D, Shaver J, Somers D and Gengenbach B (1996) Lysine accumulation in maize cell cultures transformed with a lysine-insensitive form of maize dihydrodipicolinate synthase.Theor App Genet 92: 70-77.

Blagova E, Levdikov V, Milioti N, Fogg MJ, Kalliomaa AK, Brannigan JA, Wilson KS and Wilkinson AJ (2006) Crystal structure of dihydrodipicolinate synthase (BA3935) from *Bacillus anthracis* at 1.94 A resolution. Proteins 62: 297-301.

Blickling S, Beisel HG, Bozic D, Knablein J, Laber B and Huber R (1997) Structure of dihydrodipicolinate synthase of *Nicotiana sylvestris* reveals novel quaternary structure. J Mol Biol 274: 608-621.

Blickling S, Renner C, Laber B, Pohlenz HD, Holak TA and Huber R (1997) Reaction mechanism of *Escherichia coli* dihydrodipicolinate synthase investigated by X-ray crystallography and NMR spectroscopy. Biochem 36: 24-33.

Boughton BA, Griffin MDW, O'Donnell PA, Dobson RCJ, Perugini MA, Gerrard JA and Hutton CA (2008) Irreversible inhibition of dihydrodipicolinate synthase by 4-oxo-heptenedioic acid analogues. Bioorg Med Chem 16: 9975-9983

Bradrick TD, Beechem JM and Howell EE (1996) Unusual binding stoichiometries and cooperativity are observed during binary and ternary complex formation in the single active pore of R67 dihydrofolate reductase, a D2 symmetric protein. Biochem 35: 11414-11424.

Brinch-Pedersen H, Galili G, Knudsen S and Holm PB (1996) Engineering of the aspartate family biosynthetic pathway in barley (*Hordeum vulgare L.*) by transformation with heterologous genes encoding feed-back-insensitive aspartate kinase and dihydrodipicolinate synthase. Plant Mol Biol 32: 611-620.

Burgess BR, Dobson RC, Bailey MF, Atkinson SC, Griffin MD, Jameson GB, Parker MW, Gerrard JA and Perugini MA (2008) Structure and evolution of a novel dimeric enzyme from a clinically important bacterial pathogen. J Biol Chem 283: 27598-27603.

Cahyanto MN, Kawasaki H, Nagashio M, Fujiyama K and Seki T (2006) Regulation of

aspartokinase, aspartate semialdehyde dehydrogenase, dihydrodipicolinate synthase and dihydrodipicolinate reductase in *Lactobacillus plantarum*. Microbiol 152: 105-112.

Chen VB, Arendall WB, 3rd, Headd JJ, Keedy DA, Immormino RM, Kapral GJ, Murray LW, Richardson JS and Richardson DC (2010) MolProbity: all-atom structure validation for macromolecular crystallography. Acta Crysta D66: 12-21.

Collaborative Computational Project Number 4 (1994) The CCP4 suite: programs for protein crystallography. Acta Crysta D50: 760-763.

Cornish-Bowden A (1976) Principles of enzyme kinetics. Butterworths, London .

Cox RJ, Sutherland A and Vederas JC (2000) Bacterial diaminopimelate metabolism as a target for antibiotic design. Bioorg Med Chem 8: 843-871.

Cremer J, Treptow C, Eggeling L and Sahm H (1988) Regulation of enzymes of lysine biosynthesis in *Corynebacterium glutamicum*. J Gen Microbiol 134: 3221-3229.

Davis AJ, Perugini MA, Smith BJ, Stewart JD, Ilg T, Hodder AN and Handman E (2004) Properties of GDP-mannose pyrophosphorylase, a critical enzyme and drug target in *Leishmania mexicana*. J Bioll Chem 279: 12462-12468.

Demeler B (2005a) Bioinformatics basics: Applications in biological science and medicine. In: Rashidi H , Buehler L (eds) Hydrodynamic Methods, CRC Press LLC, Florida, pp. 226-255.

Demeler B (2005b) Ultrascan: A comprehensive data analysis software package for analytical ultracentrifugation experiments. Royal Society of Chemistry, Cambridge.

Demeler B and van Holde KE (2004) Sedimentation velocity analysis of highly heterogeneous systems. Anal Biochem 335: 279-288.

Dereppe C, Bold G, Ghisalba O, Ebert E and Schar HP (1992) Purification and characterization of dihydrodipicolinate synthase from pea. Plant Physiol 98: 813-821.

Devenish SR, Gerrard JA, Jameson GB and Dobson RC (2008) The high-resolution structure of dihydrodipicolinate synthase from *Escherichia coli* bound to its first substrate, pyruvate. Acta Crystallogr Sect F Struct Biol Cryst Commun 64: 1092-1095.

Devenish SR, Huisman FH, Parker EJ, Hadfield AT and Gerrard JA (2009) Cloning and characterisation of dihydrodipicolinate synthase from the pathogen *Neisseria meningitidis*. Biochim Biophys Acta 1794: 1168-1174.

Dobson RC, Devenish SR, Turner LA, Clifford VR, Pearce FG, Jameson GB and Gerrard JA

(2005) Role of arginine 138 in the catalysis and regulation of *Escherichia coli* dihydrodipicolinate synthase. Biochemistry 44: 13007-13013.

Dobson RC, Griffin MD, Devenish SR, Pearce FG, Hutton CA, Gerrard JA, Jameson GB and Perugini MA (2008) Conserved main-chain peptide distortions: a proposed role for Ile203 in catalysis by dihydrodipicolinate synthase. Protein Sci 17: 2080-2090.

Dobson RC, Griffin MD, Jameson GB and Gerrard JA (2005) The crystal structures of native and (S)-lysine-bound dihydrodipicolinate synthase from *Escherichia coli* with improved resolution show new features of biological significance. Acta Crysta D61: 1116-1124.

Dobson RC, Valegard K and Gerrard JA (2004) The crystal structure of three site-directed mutants of *Escherichia coli* dihydrodipicolinate synthase: further evidence for a catalytic triad. J Mol Biol 338: 329-339.

Dogovski C, Atkinson SC, Dommaraju SR, Downton M, Hor L, Moore S, Paxman JJ, Pevereli MG, Qiu TW, Reumann M, Siddiqui T, Taylor NL, Wagner J, Wubben JM, Perugini MA (2012) Enzymology of bacterial Lysine biosynthesis. In: Ekinci, D (ed) Biochemistry, InTech Open Access Publisher, Rijeka, pp. 225-262.

Dogovski C, Atkinson SC, Dommaraju SR, Hor L, Hutton CA, Gerrard JA, Perugini MA (2009) Lysine biosynthesis in bacteria – an unchartered pathway for novel antibiotic design in biotechnology: Fundamentals and modern development Part I. In: Doelle, H (ed) Encyclopedia of Life Support Systems (EOLSS) Eolss Publishers, Oxford, pp. 116-136.

Domigan LJ, Scally SW, Fogg MJ, Hutton CA, Perugini MA, Dobson RC, Muscroft-Taylor AC, Gerrard JA and Devenish SR (2009) Characterisation of dihydrodipicolinate synthase (DHDPS) from *Bacillus anthracis*. Biochim Biophys Acta 1794: 1510-1516.

Emsley P and Cowtan K (2004) Coot: model-building tools for molecular graphics. Acta Crystal D60: 2126-2132.

Evans G and Pettifer RF (2001) CHOOCH: a program for deriving anomalous-scattering factors from X-ray fluorescence spectra. J Appl Crystall 34: 82-86.

Evans P (2006) Scaling and assessment of data quality. Acta Crysta D62: 72-82.

Frankard V, Ghislain M and Jacobs M (1992) Two feedback-insensitive enzymes of the aspartate pathway in *Nicotiana sylvestris*. Plant Physiol 99: 1285-1293.

Frisch DA, Gengenbach BG, Tommey AM, Sellner JM, Somers DA and Myers DE (1991) Isolation and characterization of dihydrodipicolinate synthase from maize. Plant Physiol

96: 444-452.

Galili G (1995) Regulation of Lysine and Threonine Synthesis. Plant Cell 7: 899-906.

Ghislain M, Frankard V and Jacobs M (1990) Dihydrodipicolinate synthase of *Nicotiana sylvestris*, a chloroplast-localized enzyme of the lysine pathway. Planta 180: 480-486.

Ghislain M, Frankard V and Jacobs M (1995) A dinucleotide mutation in dihydrodipicolinate synthase of *Nicotiana sylvestris* leads to lysine overproduction. Plant J 8: 733-743.

Girish TS, Sharma E and Gopal B (2008) Structural and functional characterization of *Staphylococcus aureus* dihydrodipicolinate synthase. FEBS Lett 582: 2923-2930.

Griffin MD, Dobson RC, Gerrard JA and Perugini MA (2010) Exploring the dihydrodipicolinate synthase tetramer: how resilient is the dimer-dimer interface? Arch Biochem Biophys 494: 58-63.

Griffin MD, Dobson RC, Pearce FG, Antonio L, Whitten AE, Liew CK, Mackay JP, Trewhella J, Jameson GB, Perugini MA and Gerrard JA (2008) Evolution of quaternary structure in a homotetrameric enzyme. J Mol Biol 380: 691-703.

Griffin MDW, Billakanti JM, Wason A, Keller S, Mertens HDT, Atkinson SC, Dobson RCJ, Perugini MA, Gerrard JA and Pearce FG (2012) Characterisation of the first enzymes committed to lysine biosynthesis in *Arabidopsis thaliana*. PLoS One 7: e40318.

Halling SM and Stahly DP (1976) Dihydrodipicolinic acid synthase of *Bacillus licheniformis*. Quaternary structure, kinetics, and stability in the presence of sodium chloride and substrates. Biochim Biophys Acta 452: 580-596.

Hill AV (1910) The possible effects of the aggregation of the molecules of haemoglobin on its dissociation curves. J Physiol 40 Suppl, iv-vii.

Hoganson DA and Stahly DP (1975) Regulation of dihydrodipicolinate synthase during growth and sporulation of *Bacillus cereus*. J Bacteriol 124: 1344-1350.

Humphrey W, Dalke A and Schulten K (1996) VMD: Visual molecular dynamics. J Mol Graphics 14: 33-38.

Hutton CA, Perugini MA and Gerrard JA (2007) Inhibition of lysine biosynthesis: an evolving antibiotic strategy. Mol Biosyst 3: 458-465.

Igartuburu JM, del Río RM, Massanet GM, Montiel JA, Pando E and Luis FR (1991) Study of agricultural by-products. Extractability and amino acid composition of grapeseed *(Vitis vinifera*) proteins. J Sci Food Agri 54: 489-493.

Kefala G, Evans GL, Griffin MD, Devenish SR, Pearce FG, Perugini MA, Gerrard JA, Weiss MS and Dobson RC (2008) Crystal structure and kinetic study of dihydrodipicolinate synthase from *Mycobacterium tuberculosis*. Biochem J 411: 351-360.

Krissinel E and Henrick K (2007) Inference of macromolecular assemblies from crystalline state. J Mol Biol 372: 774-797.

Kumpaisal R, Hashimoto T and Yamada Y (1987) Purification and characterization of dihydrodipicolinate synthase from wheat suspension cultures. Plant Physiol 85: 145-151.

Kwon T, Sasahara T and Abe T (1995) Lysine accumulation in transgenic tobacco expressing dihydrodipicolinate synthase of *Escherichia coli*. J Plant Physiol 146: 615-621.

Laue TM, Shah BD, Ridgeway TM, Pelletier SL (1992) Analytical ultracentrifugation in biochemistry and polymer science. p. 90-125, The Royal Society of Chemistry, Cambridge.

Leslie AGW, Powell, HR, Processing diffraction data with mosflm. (2007) In: Read RJ, Sussman JL, (eds) Evolving Methods for Macromolecular Crystallography. Springer, Dordrecht, pp. 41-51.

MacKerell AD, Bashford D, Bellott, Dunbrack RL, Evanseck JD, Field MJ, Fischer S, Gao J, Guo H, Ha S, Joseph-McCarthy D, Kuchnir L, Kuczera K, Lau FTK, Mattos C, Michnick S, Ngo T, Nguyen DT, Prodhom B, Reiher WE, Roux B, Schlenkrich M, Smith JC, Stote R, Straub J, Watanabe M, Wiórkiewicz-Kuczera J, Yin D and Karplus M (1998) All-atom empirical potential for molecular modeling and dynamics studies of proteins. Journal Phys Chem 102: 3586-3616.

Matthews BF and Widholm JM (1979) Expression of aspartokinase, dihydrodipicolinic acid synthase and homoserine dehydrogenase during growth of carrot cell suspension cultures on lysine- and threonine-supplemented media. Z Naturforsch C 34: 1177-1185.

McCoy AJ, Grosse-Kunstleve RW, Adams PD, Winn MD, Storoni LC and Read RJ (2007) Phaser crystallographic software. J Appl Crystall 40: 658-674.

McPhillips TM, McPhillips SE, Chiu HJ, Cohen AE, Deacon AM, Ellis PJ, Garman E, Gonzalez A, Sauter NK, Phizackerley RP, Soltis SM and Kuhn P (2002) Blu-Ice and the Distributed Control System: software for data acquisition and instrument control at macromolecular crystallography beamlines. J Synchrotron Radiat 9: 401-406.

Mirwaldt C, Korndorfer I and Huber R (1995) The crystal structure of dihydrodipicolinate

synthase from *Escherichia coli* at 2.5 A resolution. J Mol Biol 246: 227-239.

Mitsakos V, Dobson RCJ, Pearce FG, Devenish SR, Evans GL, Burgess BR, Perugini MA, Gerrard JA and Hutton CA (2008) Inhibiting dihydrodipicolinate synthase across species: towards specificity for pathogens? Bioorg Med Chem Lett 18: 842-844.

Murshudov GN, Vagin AA and Dodson EJ (1997) Refinement of macromolecular structures by the maximum-likelihood method. Acta Crysta D53: 240-255.

Muscroft-Taylor AC, Soares da Costa TP and Gerrard JA (2010) New insights into the mechanism of dihydrodipicolinate synthase using isothermal titration calorimetry. Biochimie 92: 254-262.

Negrutiu I, Cattoir-Reynearts A, Verbruggen I and Jacobs M (1984) Lysine overproducer mutants with an altered dihydrodipicolinate synthase from protoplast culture of Nicotiana sylvestris. Theor Appl Genet 68: 11-20.

Nicholson K, Tarlyn N, Armour T, Swanson M and Dhingra A (2012) Effect of phyllotactic position and cultural treatments toward successful direct shoot organogenesis in dwarf 'Pixie' grapevine (*Vitis vinifera L.*). Plant Cell, Tissue and Organ Culture (PCTOC) 111: 123-129.

Nunan KJ, Sims IM, Bacic A, Robinson SP and Fincher GB (1997) Isolation and characterization of cell walls from the mesocarp of mature grape berries (*Vitis vinifera*). Planta 203: 93-100.

Perl A, Shaul O and Galili G (1992) Regulation of lysine synthesis in transgenic potato plants expressing a bacterial dihydrodipicolinate synthase in their chloroplasts. Plant Mol Biol 19: 815-823.

Perugini MA, Griffin MDW., Smith BJ, Webb LE, Davis AJ, Handman E and Gerrard JA (2005) Insight into the self-association of key enzymes from pathogenic species. Eur Biophys J 34: 469-476.

Perugini MA, Schuck P and Howlett GJ (2000) Self-association of human apolipoprotein E3 and E4 in the presence and absence of phospholipid. J Biol Chem 275: 36758-36765.

Phenix CP and Palmer DR (2008) Isothermal titration microcalorimetry reveals the cooperative and noncompetitive nature of inhibition of *Sinorhizobium meliloti* L5-30 dihydrodipicolinate synthase by (*S*)-lysine. Biochem 47: 7779-7781.

Phillips JC, Braun R, Wang W, Gumbart J, Tajkhorshid E, Villa E, Chipot C, Skeel RD, Kale L

and Schulten K (2005) Scalable molecular dynamics with NAMD. J comp chem 26: 1781-1802.

Ricard, J. and Cornish-Bowden, A. (1987) Co-operative and allosteric enzymes: 20 years on. Eur. J. Biochem. 166: 255-272.

Sarrobert C, Thibaud MC, Contard-David P, Gineste S, Bechtold N, Robaglia C and Nussaume L (2000) Identification of an *Arabidopsis thaliana* mutant accumulating threonine resulting from mutation in a new dihydrodipicolinate synthase gene. Plant J 24: 357-367.

Shaul O and Galili G (1992a) Increased lysine synthesis in tobacco plants that express high levels of bacterial dihydrodipicolinate synthase in their chloroplasts. The Plant Journal 2: 203-209.

Shaul O and Galili G (1992b) Threonine overproduction in transgenic tobacco plants expressing a mutant desensitized aspartate kinase of *Escherichia coli*. Plant Physiol 100: 1157-1163.

Shaul O and Galili G (1993) Concerted regulation of lysine and threonine synthesis in tobacco plants expressing bacterial feedback-insensitive aspartate kinase and dihydrodipicolinate synthase. Plant Mol Biol 23: 759-768.

Shaver JM, Bittel DC, Sellner JM, Frisch DA, Somers DA and Gengenbach BG (1996) Single-amino acid substitutions eliminate lysine inhibition of maize dihydrodipicolinate synthase. Proc Natl Acad Sci USA 93: 1962-1966.

Silk GW and Matthews BF (1997) Soybean *dapA* mutations encoding lysine-insensitive dihydrodipicolinate synthase. Plant Mol Biol 33: 931-933.

Soares da Costa TP, Muscroft-Taylor AC, Dobson RCJ, Devenish SRA, Jameson GB and Gerrard JA (2010) How essential is the 'essential' active-site lysine in dihydrodipicolinate synthase? Biochimie 92: 837-845.

Sreerama N and Woody RW (2000) Estimation of protein secondary structure from circular dichroism spectra: comparison of CONTIN, SELCON, and CDSSTR methods with an expanded reference set. Anal Biochem 287: 252-260.

Turnbull WB and Daranas AH (2003) On the value of c: can low affinity systems be studied by isothermal titration calorimetry? J Am Chem Soc 125: 14859-14866.

van der Meer IM, Bovy AG and Bosch D (2001) Plant-based raw material: improved food quality for better nutrition via plant genomics. Curr Opin Biotechnol 12: 488-492.

Vauterin M, Frankard V and Jacobs M (2000) Functional rescue of a bacterial *dapA* auxotroph

with a plant cDNA library selects for mutant clones encoding a feedback-insensitive dihydrodipicolinate synthase. Plant J 21: 239-248.

Vauterin M and Jacobs M (1994) Isolation of a poplar and an *Arabidopsis thaliana* dihydrodipicolinate synthase cDNA clone. Plant Mol Biol 25: 545-550.

Vivier MA and Pretorius IS (2002) Genetically tailored grapevines for the wine industry. Trends Biotechnol 20: 472-478.

Voss JE, Scally SW, Taylor NL, Atkinson SC, Griffin MD, Hutton CA, Parker MW, Alderton MR, Gerrard JA, Dobson RC, Dogovski C and Perugini MA (2010) Substrate-mediated stabilization of a tetrameric drug target reveals Achilles heel in anthrax. J Biol Chem 285: 5188-5195.

Wallsgrove RM and Mazelis M (1980) The enzymology of lysine biosynthesis in higher plants: complete localization of the regulatory enzyme dihydrodipicolinate synthase in the chloroplasts of spinach leaves. FEBS Lett 116: 189-192.

Webster FH and Lechowich RV (1970) Partial purification and characterization of dihydrodipicolinic acid synthetase from sporulating *Bacillus megaterium*. J Bacteriol 101: 118-126.

Yamakura F, Ikeda Y, Kimura K and Sasakawa T (1974) Partial purification and some properties of pyruvate-aspartic semialdehyde condensing enzyme from sporulating *Bacillus subtilis*. J Biochem 76: 611-621.

Yugari Y and Gilvarg C (1965) The condensation step in diaminopimelate synthesis. J Biol Chem 240: 4710-4716.

Zhu X and Galili G (2003) Increased lysine synthesis coupled with a knockout of its catabolism synergistically boosts lysine content and also transregulates the metabolism of other amino acids in *Arabidopsis* seeds. Plant Cell 15: 845-853.

TABLES

Table 1. Kinetic Properties of *Vv*-DHDPS

With respect to pyruvate (Pyr):	
K_I^{LYS} (Pyr)	K_I^{LYS} (ES) = 0.063 ± 0.02 m*M*
	K_I^{LYS} (E) = 0.054 ± 0.01 m*M*
Apparent Hill coefficient (n_{app})[a]	1.9
*n*ES/*n*E[b]	1.0 ± 0.1/2.4 ± 0.3
With respect to ASA:	
K_I^{LYS} (ASA)	0.049 ± 0.01 m*M*
Apparent Hill coefficient (n_{app})[c]	1.7
Hill coefficient (n)[d]	1.7 ± 0.2

[a]Apparent Hill coefficient determined from Fig. 3b.

[b]Hill coefficients derived from the nonlinear best fit to a mixed inhibition model (Fig. 3a).

[c]Apparent Hill coefficient determined from Supplementary Fig. 1b.

[d]Hill coefficients derived from the nonlinear best fit to a mixed (non-competitive) inhibition model (Supplementary Fig. 1a).

Table 2. Thermodynamic parameters determined by ITC[a].

$K_d(Lys_1)$ (m*M*)	0.002 ± 0.0003
ΔH_1 (kJ/mol)	-81 ± 6.2
$T\Delta S_1$ (kJ/mol)	600
$K_d(Lys_2)$ (m*M*)	0.38 ± 0.14
ΔH_2 (kJ/mol)	-870 ± 27
$T\Delta S_2$ (kJ/mol)	340

[a]Experiments were performed by titrating lysine into *Vv*-DHDPS (initial concentration = 80 μM) at 20 °C in 200 mM HEPES 5 mM pyruvate, pH 7.7. Best fits were obtained by employing a sequential two site model.

Table 3. Data collection, processing and refinement statistics for *Vv*-DHDPS (PDB ID: 4HNN). Values in parentheses are for the highest resolution bin.

Wavelength (Å)	0.9536
No. of images	360
Step range (°)	0.5
Space group	C2
Unit cell parameters (Å)	a=220.61, b=137.93, c=133.94
Bond angles (°)	α=γ= 90.0, β=108
Resolution (Å)	52.4-2.40 (2.53-2.40)
Observed reflections	362734 (53663)
Unique reflections	146233 (21393)
Completeness (%)	98.5 (99.0)
$\boldsymbol{R}_{\mathbf{merge}}$ [a]	0.101 (0.412)
$\boldsymbol{R}_{\mathbf{r.i.m}}$ [b]	0.124 (0.505)
$\boldsymbol{R}_{\mathbf{p.i.m}}$ [c]	0.072 (0.288)
Mean I/σ (I)	9.8 (2.7)
Redundancy	2.5 (2.5)
Wilson B value	24.4
Molecules per ASU	8
$\boldsymbol{V}_{\mathbf{M}}$ **(Matthews coefficient)**	2.30
Solvent content (%)	47
$\boldsymbol{R}_{\mathbf{cryst}}$	18.4
$\boldsymbol{R}_{\mathbf{free}}$	22.0
Number of atoms	
Protein	19233
Water	1083
R.m.s.d.	
Bonds	0.01
Angles	1.20
Average B factors	
Protein	24.0

Water	27.7
Ramachandran plot, # residues (%)	
Favored region	98.2
Allowed region	1.5
Disallowed region	0.3

[a] $R_{merge} = \sum_{hkl} \sum_{i} \left| I_i(hkl) - \langle I(hkl) \rangle \right| / \sum_{hkl} \sum_{i} I_i(hkl)$.

[b] $R_{r.i.m} = \sum_{hkl} [N/(N-1)]^{1/2} \sum_{i} \left| I_i(hkl) - \langle I(hkl) \rangle \right| / \sum_{hkl} \sum_{i} I_i(hkl)$.

[c] $R_{pim} = \sum_{hkl} [1/(N-1)]^{1/2} \sum_{i} \left| I_i(hkl) - \langle I(hkl) \rangle \right| / \sum_{hkl} \sum_{i} I_i(hkl)$.

where $I_i(hkl)$ is the *i*th intensity measurement of reflection *hkl* and $\langle I(hkl) \rangle$ its average and N is the redundancy of a given reflection.

FIGURE LEGENDS

Fig. 1 Structure of DHDPS from bacteria and plants. Dihydrodipicolinate synthase from **a** *E. coli* (PDB ID: 2XYC) and b *V. vinifera* (PDB:3TUU). Figure adapted from (Atkinson, Dogovski et al. 2012).

Fig. 2 Lysine biosynthesis in plants. The biosynthesis of lysine and threonine begins with the phosphorylation of (*S*)-Aspartate by Aspartokinase to form ASA. The pathways diverge at this point with the first committed step in lysine biosynthesis, namely, the DHDPS catalyzed condensation of pyruvate and ASA to form HTPA. The enzyme DHDPS is allosterically inhibited by lysine whilst Aspartokinase is allosterically inhibited by lysine and threonine.

Fig. 3 Lysine inhibition of *Vv*-DHDPS. **a** Kinetic analyses were performed by measuring the initial velocity of *Vv*-DHDPS with respect to various concentrations of the substrate pyruvate (Pyr) and inhibitor lysine (Lys). Initial velocity data were fitted to a mixed inhibition kinetic model (Eq. 2) using ENZFITTER (Biosoft software). Each data point was measured in triplicate. **b** Hill plot using data collected at a fixed Pyr concentration of 1.2 m*M* yielding a slope (apparent Hill coefficient, n_{app}) of 1.9 (Table I).

Fig. 4 Thermostability and quaternary structure of *Vv*-DHDPS in the absence and presence of lysine. **a** Thermal denaturation of un-liganded (apo) *Vv*-DHDPS (●), enzyme in the presence of; 2.0 m*M* pyruvate (Pyr) (□), 0.5 m*M* lysine (Lys) (△) and 5 m*M* pyruvate & 1 mM lysine (◇). **b** Enhanced van Holde-Weischet integral distribution plot from extrapolation of *Vv*-DHDPS raw sedimentation velocity data shown in Supplementary Fig. 4. The corrected sedimentation coefficient is plotted against the boundary fraction for *Vv*-DHDPS (13 μ*M*) in the absence (●) and presence (○) of 1.0 m*M* lysine (Lys).

Fig. 5 Crystal structure of *Vv*-DHDPS bound to lysine. **a** Crystal structure of *Vv*-DHDPS (PDB ID: 4HNN) showing the position of inhibitory lysine molecules (orange spheres) in each allosteric site and the self-association interfaces. Two monomers come together at the tight dimer interface to form the dimeric unit, which dock at the weak dimer interface to form a

homotetramer. The asymmetric unit contained eight monomers assembled as two homotetramers. **b** Allosteric site residues of *Vv*-DHDPS. Two bound lysine molecules (Lys_1 and Lys^2) are indicated (orange).

Fig. 6 a Allosteric site residues are shown from structures derived from *Vv*-DHDPS in the absence (purple) and presence (blue) of inhibitory lysine molecules (orange). **b** Space fill representation of *Vv*-DHDPS looking onto the allosteric binding cleft in the absence of lysine. Trp78 is indicated in green. **c** Space fill representation of *Vv*-DHDPS looking onto the allosteric binding cleft in the presence of lysine (pink). Trp78 is shown in green. The binding pocket closes upon binding lysine.

Fig. 7 Molecular dynamics simulations. **a** Root mean squared deviation (RMSD) of the protein backbone for tetrameric *Vv*-DHDPS in the presence (red) and absence (black) of lysine. **b** Root mean squared fluctuation (RMSF) of the protein backbone on a chain-by-chain basis for lysine free (upper panel) and lysine bound (lower panel) MD simulations. Each trace represented in a different color is derived from separate monomers within tetrameric *Vv*-DHDPS. **c** Rotational motion of Tyr132 in the lysine free enzyme (upper panel) and lysine bound structure (lower panel) MD simulations as measured by the χ_2 (C_α-C_β-C_γ-$C_{\delta1}$) dihedral angle. Each trace presented in different colors is derived from separate monomers within tetrameric *Vv*-DHDPS. **d** Clustering of snapshots based on overall backbone conformation from a concatenated trajectory containing frames from both simulations. The clustering of snapshots was performed on one of the tight dimer units only with similar results found for the opposing tight dimer pair. Only the two most populated clusters are shown (blue 41%; red 32%). Displayed residues include Trp78, Tyr131 and Tyr132.

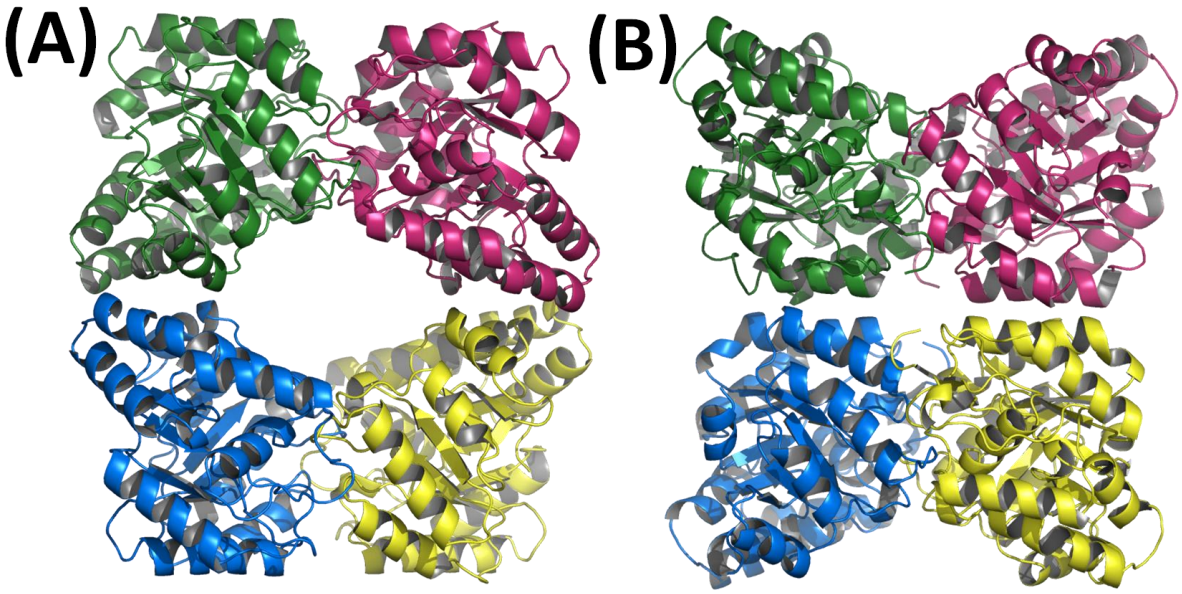
(A)
(B)

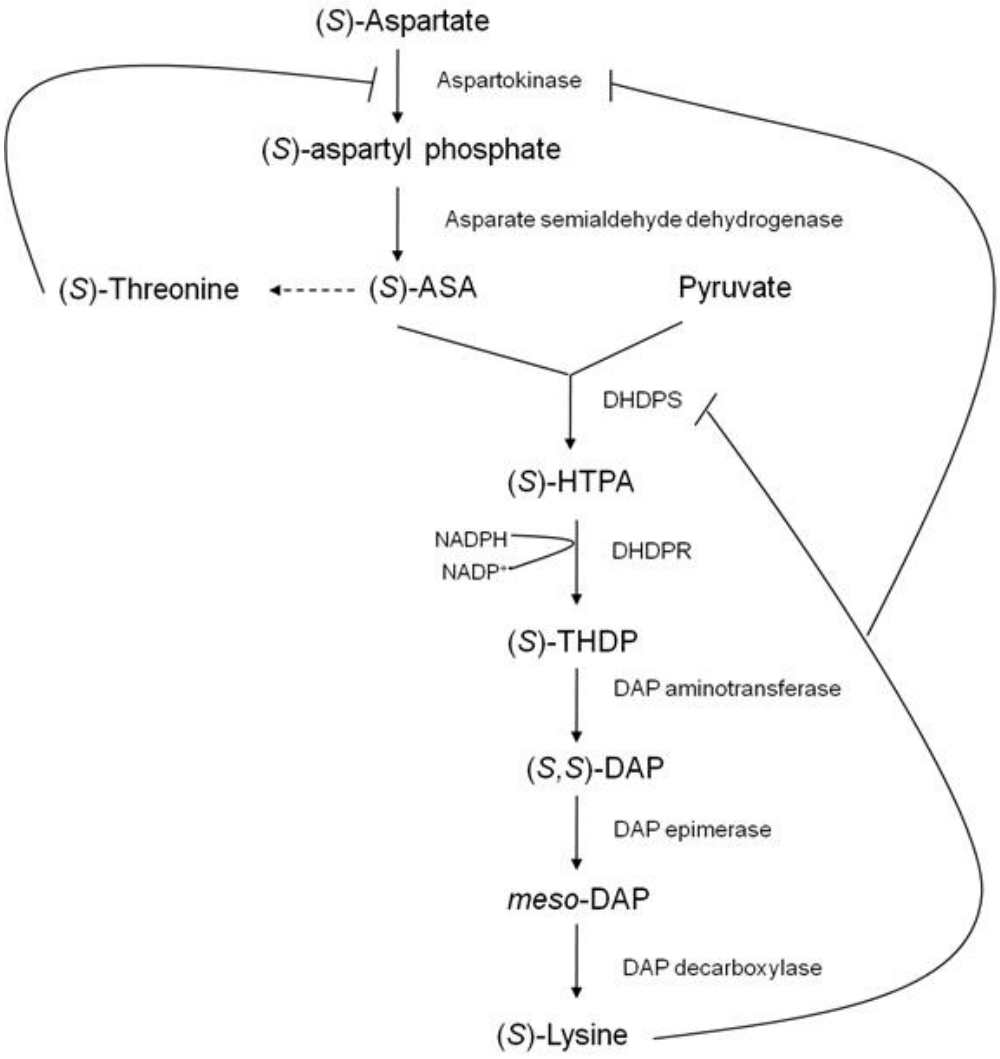
(S)-Aspartate
Aspartokinase
(S)-aspartyl phosphate
Asparate semialdehyde dehydrogenase
(S)-Threonine
(S)-ASA
Pyruvate
DHDPS
(S)-HTPA
NADPH
NADP+
DHDPR
(S)-THDP
DAP aminotransferase
(S,S)-DAP
DAP epimerase
meso-DAP
DAP decarboxylase
(S)-Lysine

(A)

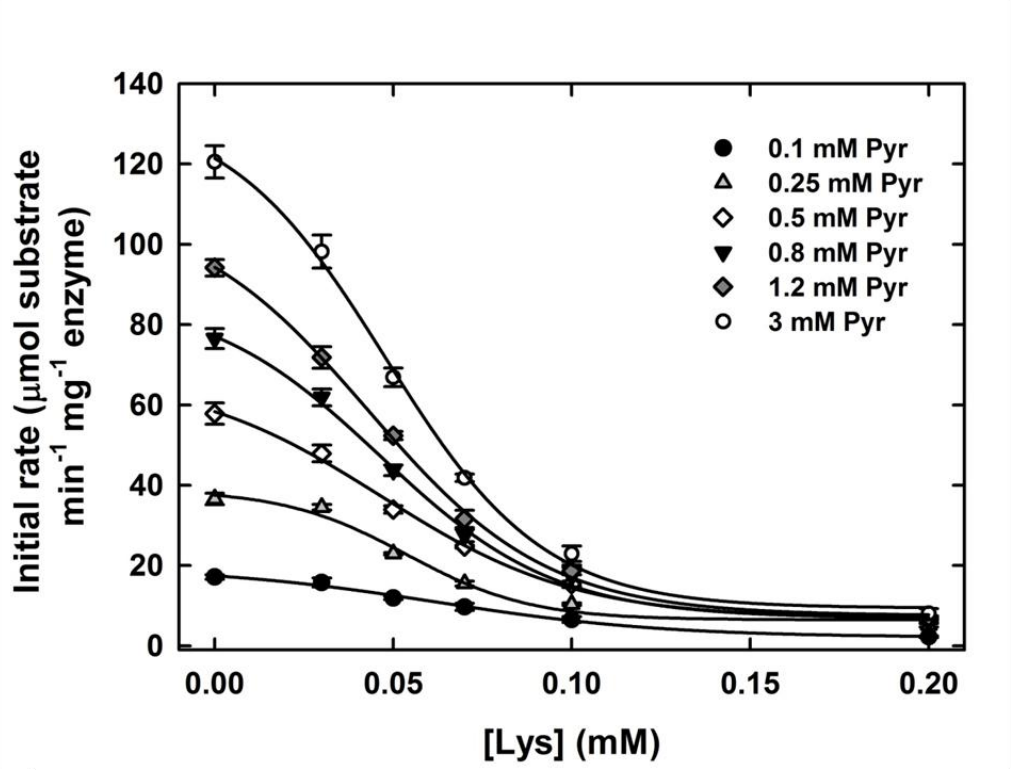
Initial rate (μmol substrate min-1 mg-1 enzyme)
[Lys] (mM)
0.1 mM Pyr
0.25 mM Pyr
0.5 mM Pyr
0.8 mM Pyr
1.2 mM Pyr
3 mM Pyr
0
20
40
60
80
100
120
140
0.00
0.05
0.10
0.15
0.20

(B)

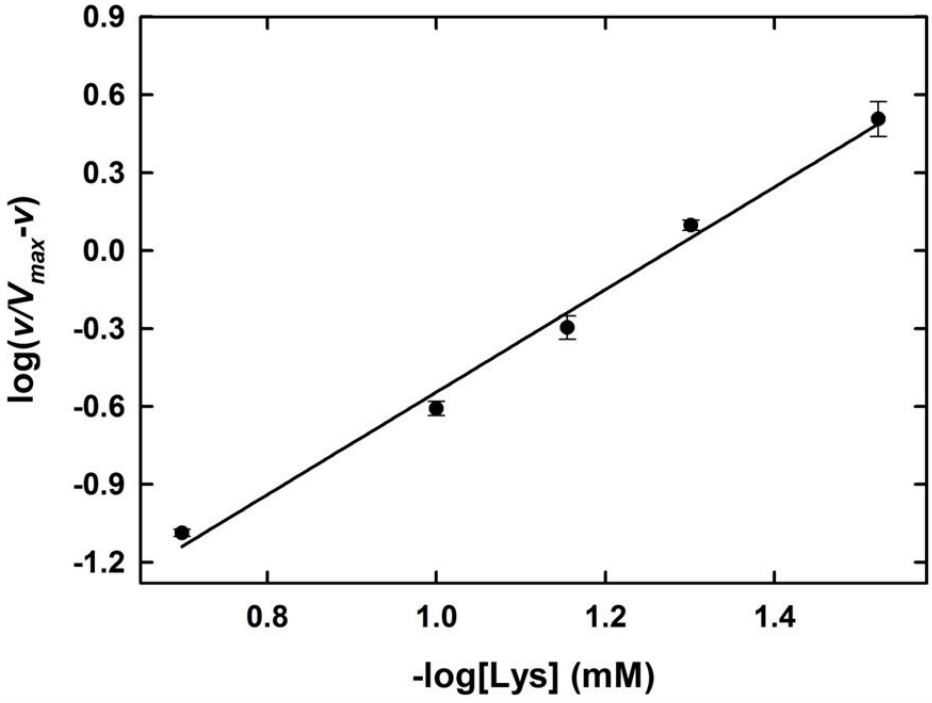
log(v/Vmax-v)
-log[Lys] (mM)
0.9
0.6
0.3
0.0
-0.3
-0.6
-0.9
-1.2
0.8
1.0
1.2
1.4

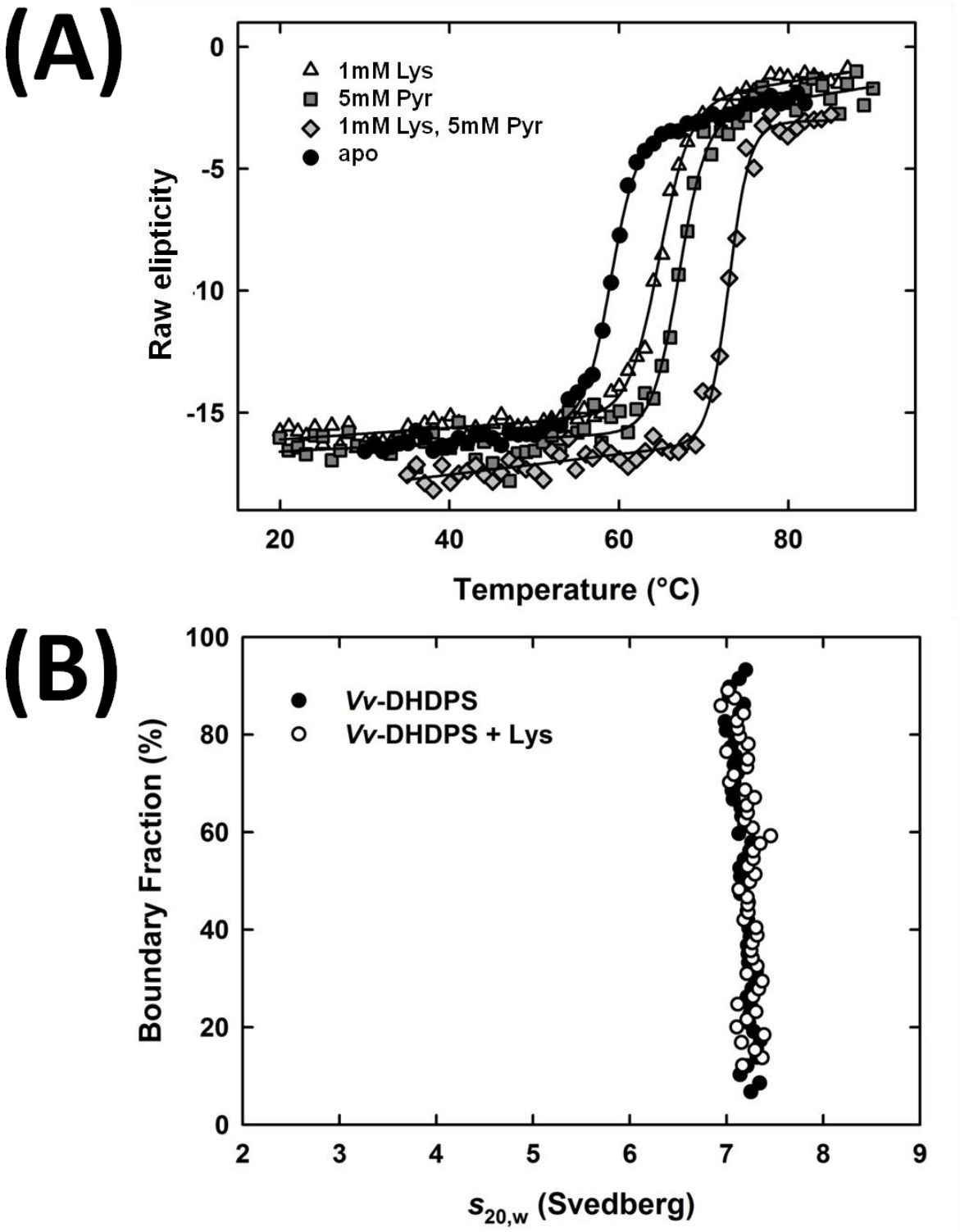
(A)
1mM Lys
5mM Pyr
1mM Lys, 5mM Pyr
apo
Raw elipticity
0
-5
-10
-15
20
40
60
80
Temperature (°C)
(B)
Vv-DHDPS
Vv-DHDPS + Lys
Boundary Fraction (%)
100
80
60
40
20
0
2
3
4
5
6
7
8
9
s20,w (Svedberg)

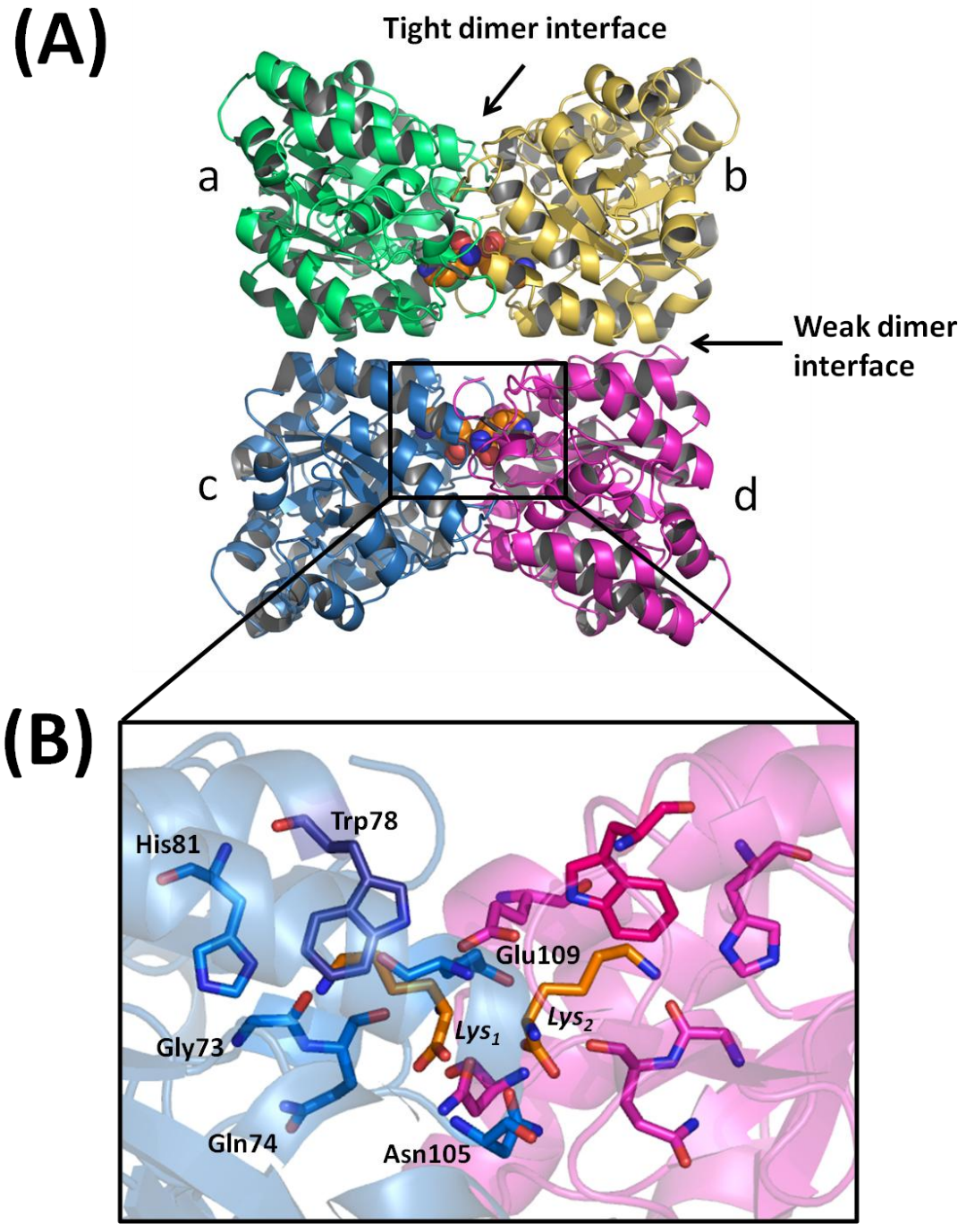
(A)
Tight dimer interface
a
b
Weak dimer interface
c
d
(B)
Trp78
His81
Glu109
Lys2
Lys1
Gly73
Gln74
Asn105

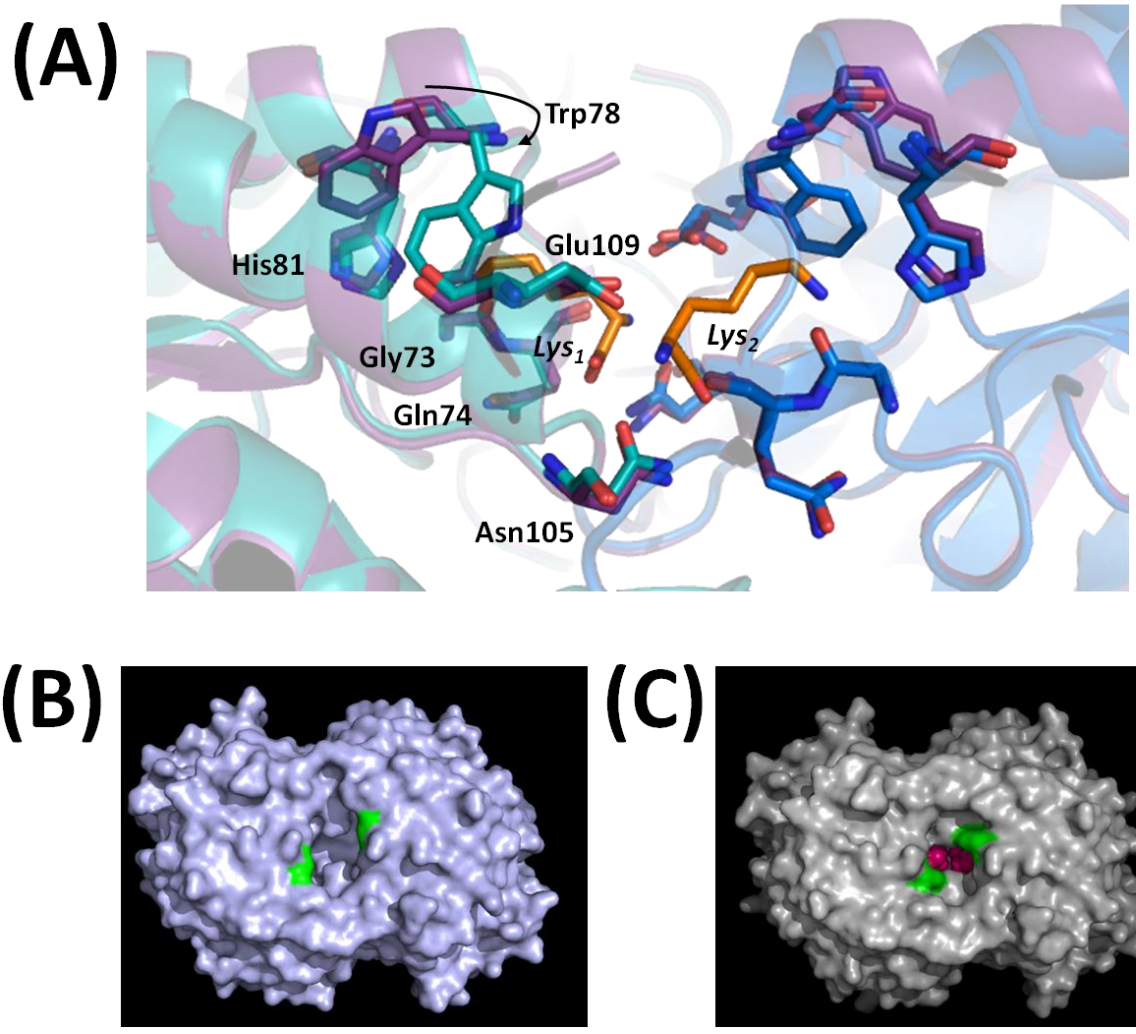
(A)
Trp78
Glu109
His81
Gly73
Lys1
Lys2
Gln74
Asn105
(B)
(C)

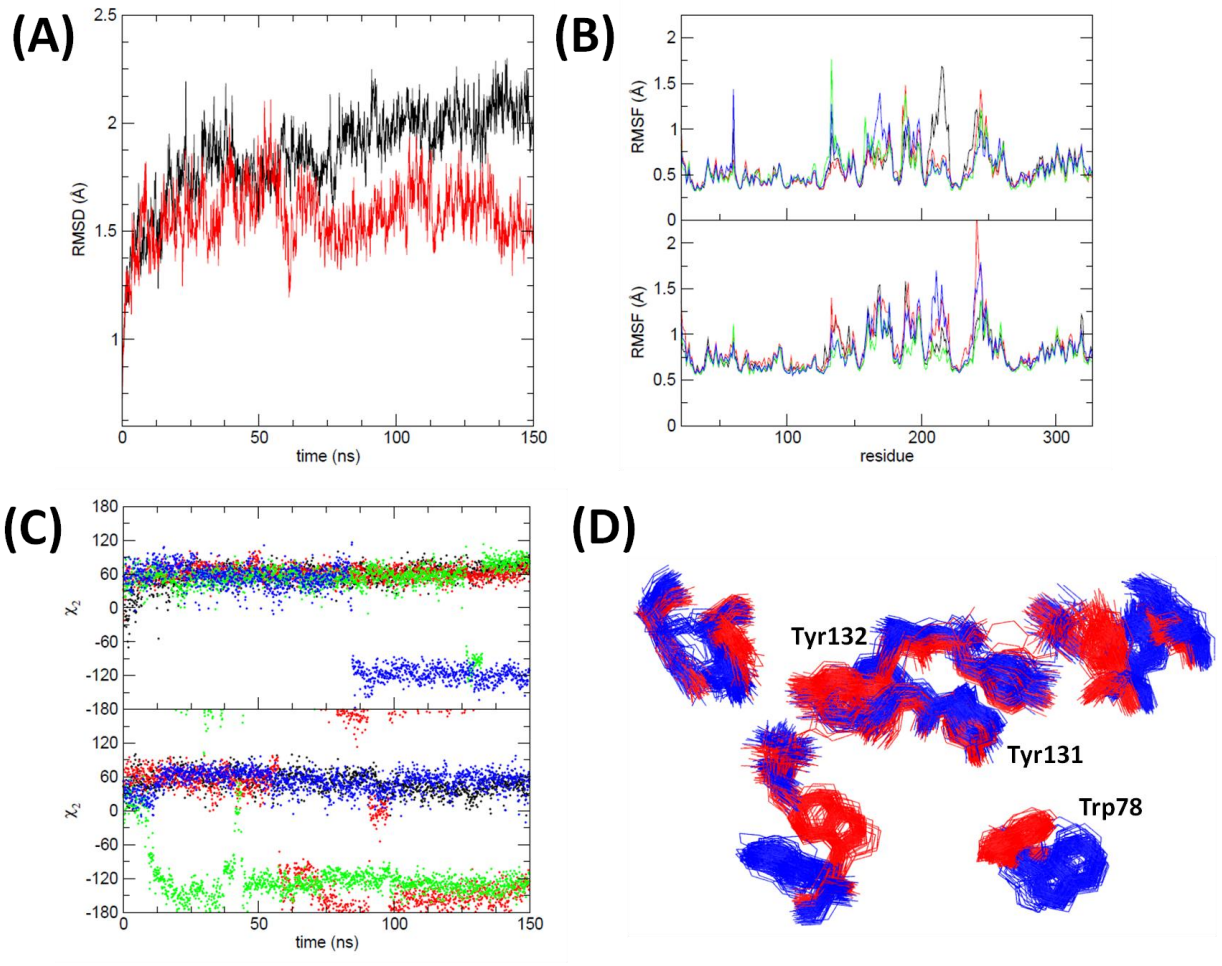
(A)
RMSD (Å)
time (ns)
(B)
RMSF (Å)
RMSF (Å)
residue
(C)
χ2
χ2
time (ns)
(D)
Tyr132
Tyr131
Trp78